UNIVERSITY OF LATVIA

Summary of Doctoral Thesis

Aigars Langins

THREE-DIMENSIONAL SIMULATIONS OF MAGNETIC FLUID FREE INTERFACE DYNAMICS USING BOUNDARY INTEGRAL EQUATIONS

Riga 2022

UNIVERSITY OF LATVIA

FACULTY OF PHYSICS, MATHEMATICS AND OPTOMETRY

Aigars Langins

THREE-DIMENSIONAL SIMULATIONS OF MAGNETIC FLUID FREE INTERFACE DYNAMICS USING BOUNDARY INTEGRAL EQUATIONS

SUMMARY OF DOCTORAL THESIS

Submitted for the degree of Doctor of Physics
Subfield of Fluid and Gas Mechanics

Scientific advisor:
Dr. habil. phys. Andrejs Cēbers

Riga, 2022

The doctoral thesis was carried out:

at the Chair of Theoretical Physics,
Department of Physics, Mathematics and Optometry
University of Latvia
from 2018 to 2022

The thesis contains an introduction, 6 chapters, reference list, 3 appendices

Form of thesis: Dissertation in Physics, subfield of Fluid and Gas Mechanics

Supervisor: prof. *Dr. habil. phys.* Andrejs Cēbers

Reviewers:

1. *Dr. phys.* Jānis Priede, Coventry University, UK,
2. *Dr.* Jānis Bajārs, University of Latvia, Latvia,
3. *Dr.* Jaakko Timonen, Aalto University, Finland.

The thesis will be defended: at public session of the Doctoral Committee of Physics, University of Latvia, at 13:30 on 16^{th} December 2022, Faculty of Physics, Mathematics and Optometry, Jelgavas 3, Riga, Latvia

The thesis is available at the Library of the University of Latvia, Raina blvd. 19.

Chairman of the Doctoral Committee: *Dr. phys.* Andris Jakovičs
Secretary of the Doctoral Committee: Sintija Siliņa

ISBN 978-9934-18-898-5
ISBN 978-9934-18-899-2 (PDF)

Abstract

This dissertation tackles the problem of describing the complex phenomena magnetic fluid droplets undergo under certain external magnetic field configurations, which has proven to be elusive of a quantitative description, except in the simplest of cases. To address this problem, a mathematical model of the full three-dimensional free surface dynamics of magnetic fluid droplets in magnetic fields is required. A particular model relying on solving boundary integral equations, as well as its algorithmic implementation is presented in this work. The algorithm can handle arbitrary droplet and carrier fluid viscosity ratios and can capture various shape instabilities the droplet might undergo under the right magnetic field conditions, like sharp conical tip development or transforming into a starfish-like form. It enables the evaluation of various approximations often used to describe ellipsoidal droplets, by comparing the droplet dynamics calculated from such approximations to the results achieved from first principles with this numerical tool. The algorithm may also be used to explore droplet configurations in arbitrary magnetic fields, as well as to indirectly calculate the physical properties of magnetic fluid droplets and to predict the magnetic field thresholds above which the droplet shape can develop surface instabilities.

Keywords: Stokes Flow, Boundary Integral, Magnetic Fluid, Instability, Equilibrium Figures.

Contents

1 Introduction

1.1 Recent developments in the field

Mathematical physics has long been concerned with equilibrium figures various objects might assume in different external physical conditions. For example, the classical problem of self-gravitating masses [1] allowed for the exploration of many bifurcations of surface shapes. The seminal paper by G.I.Taylor [2] sparked vast research into the the equilibrium shapes an electrically or magnetically responsive fluid might take, as well as their dynamics under the action of external electromagnetic fields. In particular, significant breakthrough in the research of droplets under the action of electromagnetic field arose with the synthesis of magnetic liquids [3] allowing many interesting effects to be observed and described, such as the droplet deformation and its dynamics under the action of static magnetic fields [4, 5], rotating fields [6, 7] and labyrinthine pattern formation in the Hele-Shaw cells [8, 9] or of systems of vanishing interfacial tension [10]. For the description of these effects different approximate methods [11, 12, 13] (assumption of ellipsoidal shape, satisfaction of boundary conditions on average and others) were created which need to be confirmed. Even more different observed phenomena still are not described theoretically or sufficiently explored numerically, – such as the dynamics of hysteresis of droplet deformation [14], re-entrant transition of figures of equilibrium of magnetic droplets in a high frequency rotating field [6], spike formation on the droplet's poles [15] and others. It should be noted that droplets under the action of electromagnetic field have many uses such as investigation of mechanical properties of tissue [16], dynamic self assembly [15], magnetic hyperthermia for cancer therapy [17], microrobotics for cargo transportation [18, 19], programmable droplets for flow control [20] and many others.

In parallel with the experimental investigation of magnetic droplets, significant efforts in the development of the numerical methods for their simulation have been undertaken. Efficient tools for the simula-

tion of the free boundary phenomena may be developed on the basis of the boundary integral equations [21, 22]; they have recently been used to observe various "starfish" like droplet shape instabilities in a two-dimensional Hele-Shaw cell model [23]. In axisymmetric case these methods were developed in [24, 25]. Among the phenomena predicted is, for example, the formation of the spikes on the droplet's poles if the magnetic permeability is high enough [25, 26, 27]. It may be noted that by using boundary integral equation technique the simulation of such complicated free boundary problem as the formation of the labyrinthine patterns in the Hele-Shaw cells has been carried out [28]. The application of the boundary integral equation algorithm for the real three dimensional case is a real challenge since special care should be applied to keep the quality of mesh on the the droplets surface [29, 30, 31]. Modelling such dynamics can also be approached via the level-set method [32], the immersed boundary method [33] which is sensitive to precise boundary description[34] or Lattice Boltzmann methods which can handle complex fluid configurations and the coexistence of multiple fluid phases well [35]. A further review of magnetic fluid modelling and simulations is also available [36]. In parallel to the development of the numerical tools for the simulation of magnetic droplets, corresponding elaborations are taking place for simulation of droplets in leaky dielectrics where besides the usual terms, the convective surface charge transfer by the liquid motion should be taken into account [37].

One of the first undertakings to simulate magnetic droplets in the three dimensional case was undertaken in [38] under the condition of equal viscosities of the droplet and surrounding fluid. Since the viscosities of the concentrated phase of strongly magnetic droplets obtained by the demixing of magnetic colloids are significantly larger than the viscosity of the carrier liquid (usually water) [39] it is crucial in the simulation of their dynamics to account for that in the numerical models.

At present there do not exist exact solutions of magnetic droplet behaviour under the simultaneous action of viscous, magnetic and cap-

illary forces which may be used as benchmarks for validating numerical models. In this situation the validations of the numerical models is carried out by the comparison of the numerical results with some approximate solutions. It is our aim here to carry out these comparisons using the simple model of a magnetic fluid droplet [3] using an extension of the numerical algorithm of [38].

1.2 Numerical Simulation Methods for Fluid Droplets

Magnetic fluid droplets can be investigated with optical methods, owing to their large enough dimensions, but such approaches are not as viable to measure, for example, the pressure or stress fields inside or around the droplet. In such cases numerical methods can be of great help by solving mathematical models of the underlying physical phenomena and comparing their results to experimental observations.

Integral equations allow to take into account various boundary conditions on fluid interfaces and provide a tool to relate the physical parameters like pressure, velocity, and stresses at a certain point on a particular boundary to those of all the other points on all boundaries. In this thesis we investigate the Boundary Element method (BEM), as we are particularly interested in the droplet interface dynamics and instabilities.

1.3 Main objectives of this work

Since the simulation of magnetic fluid droplets in three dimensions is still a very nascent field, especially in the case of arbitrary droplet and carrier fluid viscosity ratios, the aim of this thesis is to develop a numerical simulation tool and with it an understanding of their behaviour in various magnetic fields.

To pursue this objective, the following problems are tackled:

- Develop a three-dimensional numerical algorithm for calculation of magnetic field and velocity field of fluids based on the boundary element method relying on boundary integral equations.

- Use the algorithm to probe the limits of various approximations, often used in this setting, e.g. the assumption of the elliptical form of the droplet.
- Numerically analyze droplet shape instability onsets and evolution, e.g. the "starfish" instability.
- Apply the algorithm to indirectly obtain physical properties (surface tension, magnetic permeability and viscosity) of droplets by fitting simulation results to experimental data.
- Numerically observe previously unseen effects, e.g. the back-and-forth motion of magnetic liquid droplet in a rotating field.

1.4 Approbation of the results

1.4.1 Publications

A. Langins, A. P. Stikuts, A. Cēbers, "*A three-dimensional boundary element method algorithm for simulations of magnetic fluid droplet dynamics*", **Physics of Fluids** 34, 062105 (2022).

1.4.2 Conferences

A. Langins, A. P. Stikuts, A. Cēbers, "*A 3D BEM algorithm for simulations of magnetic fluid droplet dynamics*", **International Conference on Magnetic Fluids**, Paris, France 2019.

A. Langins, A. P. Stikuts, A. Cēbers, "*Starfish instability evolution of magnetic fluid droplets in rotating magnetic field*", **11th LIQUID MATTER CONFERENCE**, remotely in Prague, Czech Republic, 2020/2021.

1.4.3 Scientific project

European Union's Horizon 2020 research and innovation program under Grant Agreement MAMI No. 766007, "Magnetism and Microhydrodynamics".

2 Mathematical model

We consider a droplet of magnetic fluid of permeability μ suspended in an infinite non-magnetic carrier fluid and subjected to an external magnetic field. The inertia of the fluid is assumed to be negligible. In this case the motion is governed by the Stokes equations for a magnetic fluid [3, 40].

$$-\boldsymbol{\nabla} p + \eta \Delta \boldsymbol{v} + \boldsymbol{f_M} = \boldsymbol{0}, \qquad \boldsymbol{\nabla} \cdot \boldsymbol{v} = 0, \tag{1}$$

where p is the pressure, η is the dynamic viscosity, $f_{Mi} = \partial_k T_{ik}$ is the volume force due to magnetic field, and $T_{ik} = -\frac{1}{2}\mu_0 H^2 \delta_{ik} + H_i B_k$ is the Maxwell stress tensor, $\boldsymbol{H}$ is the magnetic field intensity, $\boldsymbol{B} = \mu_0(\boldsymbol{H} + \boldsymbol{M})$ is the magnetic field induction and $\boldsymbol{M}$ is the magnetization. The boundary conditions for forces on the droplet surface read

$$(\sigma_{ik}^{(e)} - \sigma_{ik}^{(i)})n_k + (T_{ik}^{(e)} - T_{ik}^{(i)})n_k - \gamma(k_1 + k_2)n_i = 0, \tag{2}$$

where $\sigma_{ik} = -p\delta_{ik} + \eta\left(\partial_i v_k + \partial_k v_i\right)$ is the stress tensor of the fluid, $\gamma(k_1 + k_2)$ is the capillary force due to the surface tension, with γ being the surface tension and k_1, k_2 being the principal surface curvatures, and $\boldsymbol{n}$ is the unit normal vector pointing out of the droplet. The superscripts (e) and (i) denote the parameters outside and inside of the droplet, respectively.

In order to determine the behaviour of the magnetic fluid droplet, the magnetic fields needs to be known on its surface. As the involved magnetic field reacts to the changes of the droplet shape momentarily, the problem can be assumed to be governed by magnetostatics.

Several assumptions are to be made in order to make the problem tractable. The droplet is assumed to be linearly magnetizable $\boldsymbol{M} = \chi \boldsymbol{H}$ where $\boldsymbol{M}$ is its magnetization, χ is the magnetic susceptibility. We also assume the involved fluids to be non-conductive and so their free current densities $\boldsymbol{J}$ to be zero – the relevant Maxwell's equation then reads $\boldsymbol{\nabla} \times \boldsymbol{H} = \boldsymbol{J} = 0$.

In this case the magnetic field can be expressed as a gradient of magnetic scalar potential $\boldsymbol{H} = \boldsymbol{\nabla}\psi$. These assumptions allow us to

conclude that the magnetic potential has to satisfy the Laplace equation $\Delta\psi = 0$.

2.1 Dimensionless equations of motion in integral form

To simplify the problem, we introduce the length scale as the radius of a spherical droplet R_0, time scale defined by $t_0 = R_0\eta^{(e)}/\gamma$, a magnetic field scale given by the external field H_0, a magnetic permeability scale given by the vacuum constant μ_0, a viscosity parameter $\lambda = \eta^{(i)}/\eta^{(e)}$ and the Bond magnetic number $Bm = 4\pi\mu_0 R_0 H_0^2/\gamma$.

Using these scales, it is possible to write an integral equation for the velocity of the points on the droplet's surface, which automatically satisfies the boundary conditions [22]:

$$\begin{aligned} v_k(\boldsymbol{y}) = &- \frac{1}{1+\lambda}\frac{1}{4\pi}\int_S (k_1(\boldsymbol{x}) + k_2(\boldsymbol{x}))n_i(\boldsymbol{x})G_{ik}(\boldsymbol{x},\boldsymbol{y})dS_x \\ &+ \frac{1}{1+\lambda}\frac{1}{4\pi}\int_S f_M(\boldsymbol{x})n_i(\boldsymbol{x})G_{ik}(\boldsymbol{x},\boldsymbol{y})dS_x \\ &+ \frac{1-\lambda}{1+\lambda}\frac{1}{4\pi}\int_S v_i(\boldsymbol{x})T_{ijk}(\boldsymbol{x},\boldsymbol{y})n_j(\boldsymbol{x})dS_x \\ &+ \frac{2}{1+\lambda}v_{0k}(\boldsymbol{y}), \end{aligned} \tag{3}$$

where the integrals are evaluated over the surface of the droplet and contain the so-called *stokeslet*, that describes the linear relation between a point force $\boldsymbol{g}$ and the velocity $\boldsymbol{v}$, given by $G_{ik}(\boldsymbol{x},\boldsymbol{y}) = \frac{\delta_{ij}}{|\boldsymbol{x}-\boldsymbol{y}|} + \frac{(x_i-y_i)(x_j-y_j)}{|\boldsymbol{x}-\boldsymbol{y}|^3}$ and the so-called *stresslet*, relating the point force and the stress tensor, given by $T_{ijk}(\boldsymbol{x},\boldsymbol{y}) = -6\frac{(x_i-y_i)(x_j-y_j)(x_k-y_k)}{|\boldsymbol{x}-\boldsymbol{y}|^5}$, and f_M is the magnetic normal force $f_M = \frac{Bm}{8\pi}(\mu-1)\left(\mu {H^{(i)}}_n^2 + {H^{(i)}}_t^2\right)$.

3 Numerical Algorithm

The magnetic fluid droplet surface is tessellated by a mesh of triangular boundary elements with collocation points (nodes) at their vertices (Figure 1). The integrals are calculated using the trapezoid integration method using only the integrand function values at the nodes. This approach allows us to conveniently recast the summation over the flat triangles to a summation over nodes [29]

$$\int_S f(\boldsymbol{x}) dS \approx \sum_i f(\boldsymbol{x}_i) \Delta S_i, \tag{4}$$

where the summation is done over every node i, and $\Delta S_i = 1/3 \sum \Delta S$ is the mean area of the triangles adjacent to the i-th node. Using this reformulation, the integral equations become simply linear systems of equations that can be solved with common numerical libraries.

The original spherical mesh is obtained by iteratively "slicing" an icosahedron, by adding more nodes on its faces and projecting the newly added nodes on a sphere, as also proposed by [41]. The simulations usually utilized two or three slicing iterations, increasing the number of nodes up to 162 or 642 respectively. The normals and the surface curvatures at each vertex are determined by fitting a paraboloid on the relevant vertex and its immediate neighboring vertices [29].

3.1 Mesh maintenance

In general, the droplet surface has a nonuniform velocity distribution, so just translating the initially uniformly distributed nodes would degrade the mesh quality rather fast, as some triangles would become more deformed than others.

To diminish this unwanted effect, numerous mesh maintenance techniques are used during the simulations, which are explained in this section.

3.1.1 *Passive* stabilization

Given that the dynamics of the droplet surface is determined solely by the normal velocity component, the mesh degradation may be slowed by properly adjusting the tangential velocity components. In the so called *passive* stabilization [30], the tangential components can be adjusted in order to minimize a certain "kinetic energy" function

$$F = \sum_{\boldsymbol{x}_{ij}} \left[\frac{d}{dt} \left(\frac{|\boldsymbol{x}_{ij}|^2}{h_{ij}^2} + \frac{h_{ij}^2}{|\boldsymbol{x}_{ij}|^2} \right) \right]^2 + 0.4 \sum_{\Delta} \frac{1}{C_\Delta^2} \left(\frac{dC_\Delta}{dt} \right)^2, \qquad (5)$$

where the first sum pertains to edges between nodes i and j and tries to keep the edges $\boldsymbol{x}_{ij}$ at some optimal length h_{ij} that is determined by the local curvatures of each node [30], while the second sum pertains to the mesh surface triangles and attempts to keep the triangles as regular as possible, by using the "compactness" of a triangle

$$C_\Delta = \frac{S_\Delta}{a^2 + b^2 + c^2}, \qquad (6)$$

with a, b, c representing the triangle side lengths, as a guide [30].

3.1.2 *Active* stabilization

The algorithm outlined above slows the mesh degradation but does not stop it entirely. In addition the so called *active* stabilization [30] between the time-stepping of nodes is necessary. In *active* stabilization the nodes are translated along the surface of the droplet in order to attempt to minimize a "potential energy" function

$$E = \sum_{\boldsymbol{x}_{ij}} \left[\frac{1}{2} \left(\frac{|\boldsymbol{x}_{ij}|^2}{h_{ij}^2} + \frac{h_{ij}^2}{|\boldsymbol{x}_{ij}|^2} \right) \right]^{50} + \sum_{\Delta} \left(\frac{C_\Delta^{reg}}{C_\Delta} \right)^{100}, \qquad (7)$$

where $C_\Delta^{reg} = \sqrt{3}/12$ is the compactness value of a regular triangle. This "potential energy" function E takes on large values when an edge $\boldsymbol{x}_{ij}$ differs a lot from its optimal length of h_{ij} and so it avoids both inappropriate crowding and scattering of vertices, as well not allowing

triangles to deviate a lot from the optimal compactness value of a regular triangle.

The above energy functions E and F have their gradients expressible in an explicit analytical form, allowing for efficient calculations.

3.1.3 Edge flipping

Edges between vertices can be reconnected. These edge flips allow for increasingly regular triangles and they are applied sequentially to all of the edges until no more flips are allowed. There are extra rules, however — an edge will not be flipped, if it would result in a node with less than five connected neighbouring nodes. This is enforced to ensure that a general paraboloid, requiring five parameters describing its shape, can be fitted to every node and its neighbors. The edge flipping algorithm is applied at every simulation step. If any edge has been flipped, *active* stabilization will be applied again to ensure the regularity of the mesh.

3.1.4 Node addition

It was found that to ensure accurate results, more nodes are needed in regions of high surface curvature, therefore, we also implement a node addition routine. However, this significantly increases the time of computation, which scales approximately as $O(N^2)$, where N is the number of nodes.

If the surface curvature is determined to be large enough with respect to some cut-off criterion ε, the new nodes would be introduced at the middle of each edge of the marked triangles [31]. These new nodes are then mutually connected so that each of them has at least five neighbours.

Finally, the neighborhood of triangles affected by this new node addition is also *actively* stabilized, similarly as in [31]. The node addition routine is shown in Figure 1.

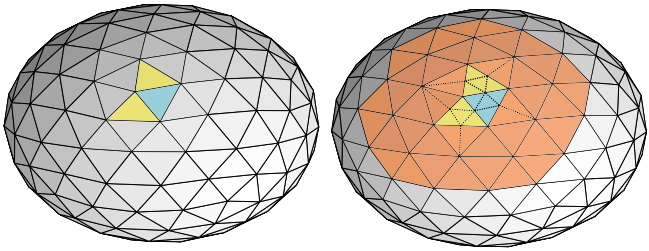

Figure 1: An illustrative example of the node addition routine. First, the triangles marked for node addition are found, as shown in yellow. As the cyan triangle has at least two neighboring triangles marked for splitting, it itself is also marked. The new nodes are added in the middle of every edge of the marked triangles, remembering to introduce extra edges to make sure every node has at least five neighbors. The new edges are indicated by the dashed lines. Finally, the affected triangles as well as their neighborhood, marked in orange, are *actively* stabilized to enhance the mesh quality.

3.2 Summary

The numerical algorithm can be briefly summarized as follows:

- For a particular external magnetic field, solve the boundary integral equation for the magnetic potential ψ on the droplet surface.
- Find the tangential H_t and normal H_n magnetic field components.
- Calculate the normal magnetic surface forces $\boldsymbol{f_M}$.
- Obtain the velocities of each node from the integral equation (3) and translate them accordingly with the first-order Euler method.
- Apply mesh maintenance techniques at every simulation step.

4 Algorithm validation

Having introduced the algorithm itself and its mesh stabilization techniques, we now turn to validating its outputs with multiple known theoretical relationships for magnetic fluid droplet equilibrium configurations and dynamics. Discrepancies between these theoretical relations and our numerical simulation results might hint at the limits of applicability of the relations themselves or the limits of the assumptions underlying their derivations.

4.1 Relaxation to a sphere

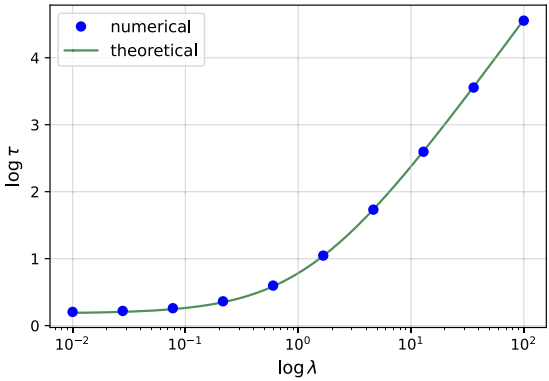

Figure 2: Characteristic dimensionless relaxation time τ of an elongated droplet as a function of the droplet-fluid viscosity ratio λ.

In the absence of an external magnetic field, the deformation of a stretched droplet, approximated with an ellipsoid of rotation, should decay exponentially under the action of capillary forces $e^{-t/\tau}$, where τ is the characteristic relaxation time.

A comparison with the numerically determined relaxation times is presented in Figure 2.

4.2 Equilibrium elongation in constant field

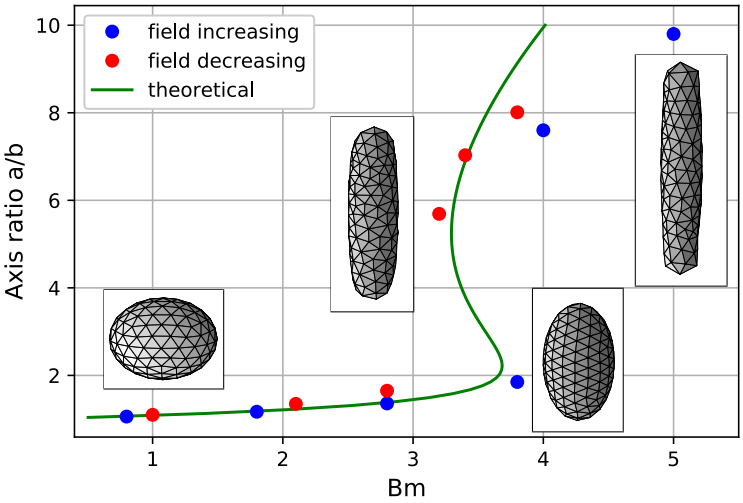

Figure 3: Evolution of the droplet through the hysteresis region. The blue (red) points indicate the calculated trajectory with increasing (decreasing) magnetic field once the droplet has equilibriated. The simulation utilized $\mu = 30$ and $\lambda = 7.6$.

We can also compare the droplet equilibrium configurations in a magnetic field determined by the algorithm against theoretical relations given below. Figure 3 exhibits the comparison between the numerically obtained equilibrium shapes of the droplet in a given magnetic field Bm with the theoretical relationship from [5, 12]

$$Bm = \left[\frac{4\pi}{\mu - 1} + N\right]^2 \frac{1}{2\pi} \frac{\left(\frac{3-2e^2}{e^2} - \frac{(3-4e^2)\arcsin e}{e^3(1-e^2)^{1/2}}\right)}{(1-e^2)^{2/3}\left(\frac{(3-e^2)}{e^5}\log\left(\frac{1+e}{1-e}\right) - \frac{6}{e^4}\right)}, \qquad (8)$$

where e symbolizes the eccentricity of the fitted ellipsoid $e = \sqrt{1 - b^2/a^2}$ with a, b being its long and short semi-axis, respectively, and N is the demagnetizing factor.

The derivation of the equilibrium formula (8) relies on an assumption of an axisymmetric ellipsoidal droplet, an approximation which works well until the axial ratio of about 7 [42]. This limit can also be observed in Fig. 3 where the simulated result deviates for highly elongated droplets, an effect explained by the droplet developing more conical tips than a fitted ellipsoid would possess at the corresponding elongation, and thus no longer obeying to the ellipsoidal approximation.

Figure 3 also shows the droplet undergoing hysteresis in its elongation whereby it might suddenly stretch when the field is increased past the critical value of about $Bm_c \approx 3.68$, but its elongation with follow a different trajectory when the field is decreased.

4.3 Elongation of quasi-stable droplets

The smaller the amount the magnetic field is over the critical value Bm_c, the longer the droplet will stay in this quasi-stable state, before it "jumps" over to a truly stable configuration, indicating a time bottleneck region.

The dynamics of this instability "jump" are governed by a hyperbolic differential equation shown by [14] for small t

$$\frac{a}{b} - \left(\frac{a}{b}\right)_c = S\ \tau \tan \frac{t}{\tau}, \tag{9}$$

where a/b is semi-axial length ratio, here τ is the characteristic time spent in the bottleneck region before the "jump", t represents time, S is a numerical constant, and the subscript c indicates critical value, i.e. the one at the extremum of the equilibrium curve (8).

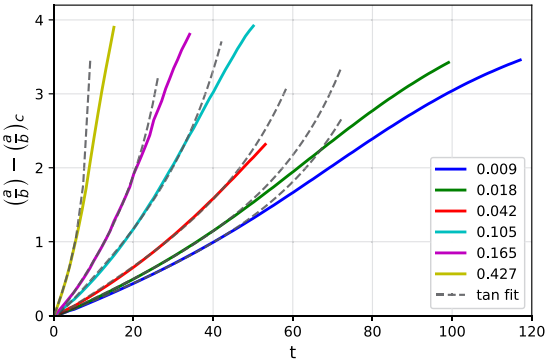

Figure 4: Elongations of the droplet during "jumping over" the hysteresis region at various external magnetic field h values, with an overlay of dashed tangential fits, according to (9). The originally accelerated dynamics saturate as the droplet reaches its new equilibrium elongation. Droplet parameter values used in simulations here were $\mu = 30, \lambda = 7.6$.

An example of multiple droplet stretching trajectories at different magnetic fields $h = H/H_c - 1$ is shown in Figure 4, with the corresponding tangential fits of Eq. (9) of τ and S overlayed with the dashed lines.

A further analysis explores the numerically obtained bottleneck behaviour of the droplet close to the critical field parameter Bm_c before "jumping" over the instable region to a stable configuration. The time spent in this bottleneck is expected to follow $\tau \sim \frac{1}{\sqrt{h}}$ [14], or $\log \tau \sim -0.5 \log h$ in logarithmic terms, which is in excellent agreement with the value of $k = -0.534$ determined from the numerical simulations.

5 Simulations

This section surveys the various simulations performed by the newly developed algorithm that, to our best knowledge, have not been done before.

The simulations of a droplet in a constant field yield two important results. First, the algorithm is able to capture the conical tip development of highly magnetic droplets.

And second, the simulated droplet shapes in increasing magnetic field strengths once the droplets have equilibriated are comparable with the shape evolution that has been observed experimentally. This comparability with experimental results allows for indirect inference of droplet parameters like viscosity, permeability and surface tension, which has previously been rather difficult for microscopic magnetic fluid droplets.

In the case of a rotating field, three notable results have been achieved. First, back-and-forth motion of a liquid object – magnetic fluid droplet – has been simulated in three dimensions. This effect has been previously observed in solid magnetic rods and elastic magnetic filaments.

Second, the development of the "starfish" instability has been numerically captured and the critical field at which this instability arises has been determined from the droplet shape evolution as well.

Finally, the simulations qualitatively point to a re-entrant transition whereby a droplet that has undergone an oblate-prolate transition in increasing magnetic field strengths will revert back to an oblate shape in even higher fields.

5.1 Constant field

5.1.1 Conical tip development

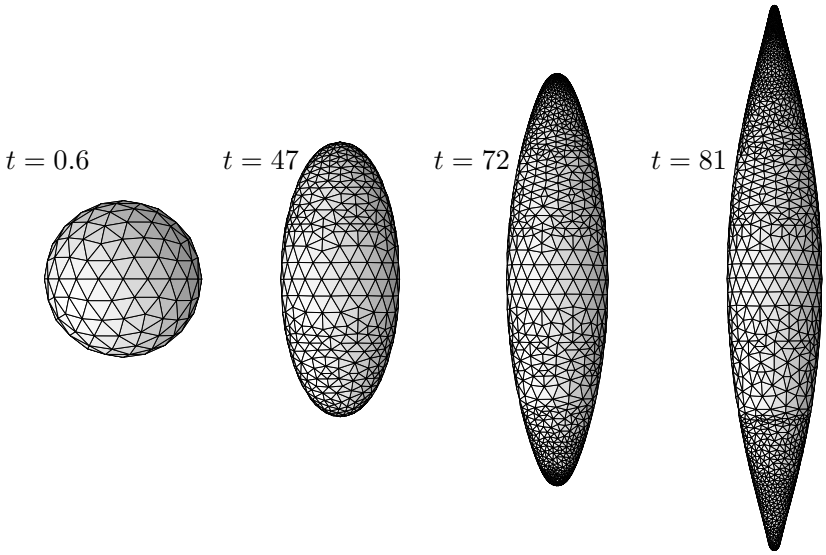

Figure 5: Droplet elongation in a constant magnetic field with $Bm = 5,\ \mu = 30,\ \lambda = 10$. Development of sharp tips can be seen, as well as addition of nodes in regions of high surface curvature. This figure has been obtained in collaboration with A. P. Stikuts.

An initially spherical magnetic fluid droplet is subjected to a constant homogeneous magnetic field and it stretches at a some rate until it reaches an equilibrium elongation, where the magnetic forces balance the surface tension force. For droplets of high magnetic permeability μ at high enough magnetic fields, it is possible for them to even grow sharp conical tips. A similar effect has been predicted [25] and observed [5] before. Here we are able to recapture this phenomenon numerically, as shown by simulation results in Figure 5.

5.1.2 Comparison with droplet elongation in experiments

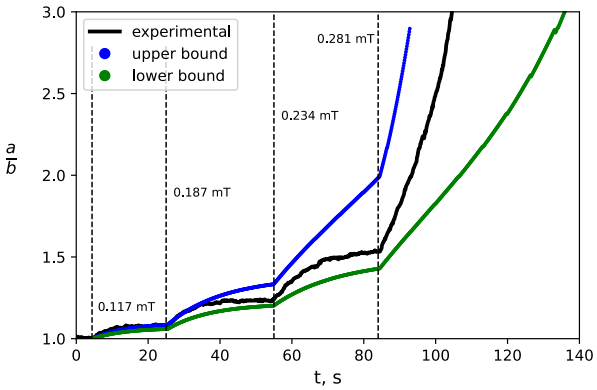

Figure 6: Stretching of a magnetic fluid droplet in a magnetic field, increasing from zero in a stepwise manner, indicated by the dotted lines. In black – experimental results with $\mu = 34 \pm 1.5$, $\gamma = (8.2 \pm 0.4) \cdot 10^{-7} J/m^2$, $\lambda = 10.1 \pm 2.5$) in an external magnetic field. The blue and green curves are obtained numerically with ($\mu = 34$, $\gamma = 7.7 \cdot 10^{-7} J/m^2$, $\lambda = 7.6$) and ($\mu = 34$, $\gamma = 8.2 \cdot 10^{-7} J/m^2$, $\lambda = 7.6$), respectively. The numerically calculated curves allow to indirectly find the bounds of the droplet parameter values. Experimental data supplied by A.P. Stikuts.

An example of a magnetic fluid droplet elongation measured experimentally is shown in Figure 6, where an initially spherical droplet is subjected to homogeneous magnetic fields of increasing magnitude in a stepwise manner. The simulation results enclose the experimental elongation curve from below and above – this would indirectly hint at the underlying bounds of droplet parameters like their surface tension γ, magnetic permeability μ and the ratio of viscosities λ.

Nonetheless, we should mention that these calculations require large computational resources and since there are three parameters to be estimated, this approach of droplet parameter estimation does not seem practical at the moment.

5.2 Rotating field

5.2.1 Back–and–forth motion

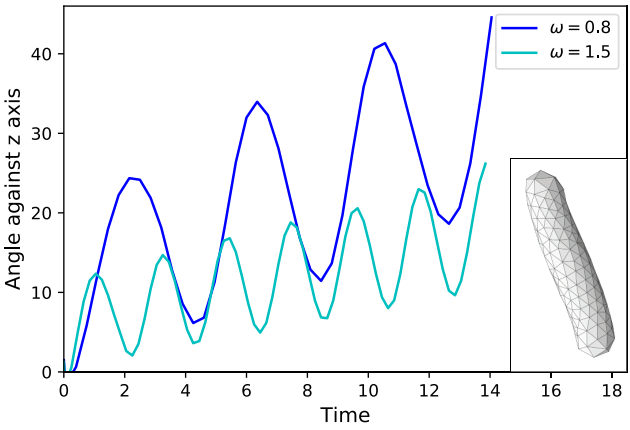

Figure 7: Back–and–forth motion of a droplet (shown in the inset), that has been first elongated in a constant magnetic field, in moderately fast rotating fields of different dimensionless frequencies ω. The curves represent the angle between longest droplet axis and the stationary z axis. Parameters used in simulations: $\mu = 30, Bm = 10, \lambda = 1$. Here node addition was disabled, to speed up the simulations.

Droplets that were initially elongated in a constant field were then exposed to a rotating magnetic field of various dimensionless frequencies ω.

At small rotation frequencies, the droplet follows the external magnetic field, as expected. However, at larger frequencies, a back-and-forth motion of the liquid droplet was observed, as seen in Figure 7 where the angle of the longest droplet axis is shown to be oscillating around an averaged uniform rotation with respect to the z axis.

5.2.2 The “starfish” instability

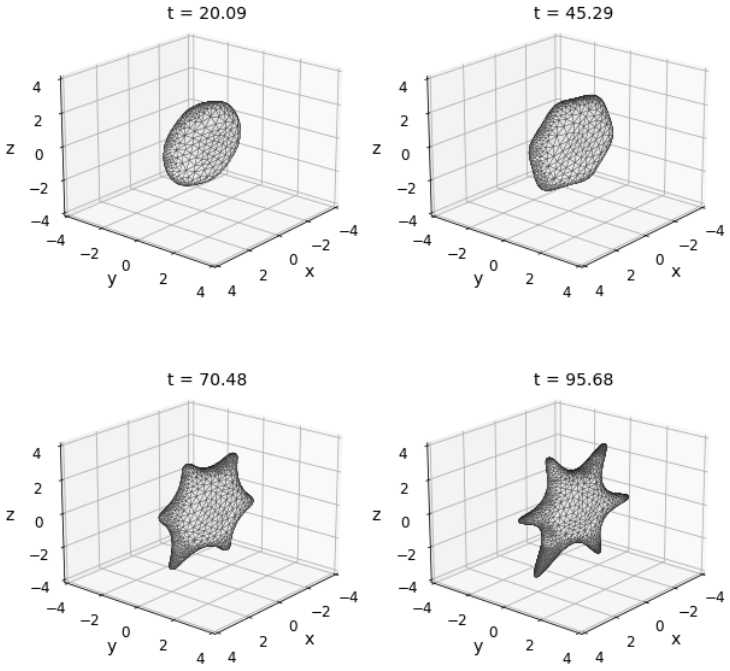

Figure 8: Example of the starfish instability developing in a rotating magnetic field, using $Bm = 35,\ \mu = 10,\ \omega = 10,\ \lambda = 7.6$ and the node addition cut-off criteria $\varepsilon = 0.4$.

The algorithm gives us the ability to explore the beginning of the starfish instability, exemplified in Figure 8. It is known to occur at fast enough and strong enough rotating magnetic fields, when the oblate magnetic fluid droplet “grows” finger–like structures around its perimeter [6].

It is possible to analyze the onset and evolution of these “starfish” instability modes by exploring how their Fourier amplitudes $A_n \propto e^{\beta_n t}$ and their logarithmic growth increments β_n behave in time at different magnetic fields.

To determine the critical field Bm_c above which a mode might manifest itself, one has to find the magnetic field value at which the slope (logarithmic increment) β of the log-amplitude evolution changes sign.

A particularly interesting mode to investigate is the $n = 2$ mode, whose growth would indicate the oblate-prolate transition, or, in possibly more relatable terms, pancake-like shape to rugby-ball-like shape transition.

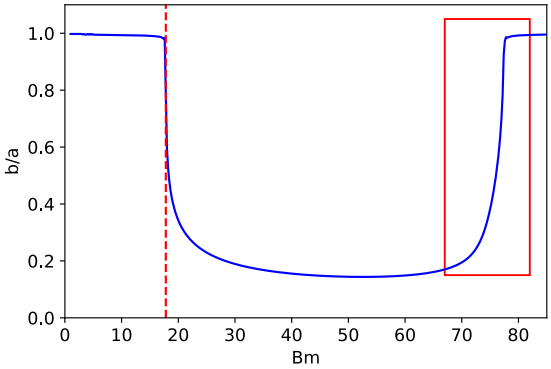

Figure 9: The vertical red line on the left side of figure shows the critical field determined via the logarithmic increment β_2 changing sign. It matches perfectly with the theoretical value. The square area on the right side of the figure shows the droplet becoming oblate (pancake-like) again at larger magnetic fields. Simulated using $\mu = 10$.

This transition is indicated by the sharp drop of the blue curve in Figure 9. The blue curve been calculated numerically by minimizing the energy of a droplet, presumed to be ellipsoidal [7, 38]. The critical field of the transition found by analyzing the behaviour of β_2 with increasing magnetic fields (shown in dashed red in Figure 9) matches very closely to the energy minimization prediction.

5.2.3 Re-entrant transition

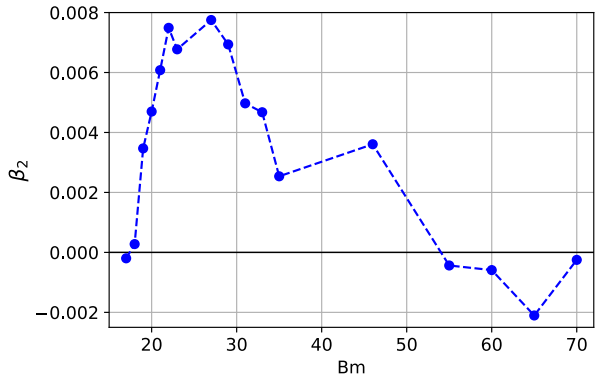

Figure 10: The logarithmic increment of the starfish mode $n = 2$ of a droplet with $\mu = 10$ becomes positive at $Bm \approx 18$, indicating a transition to a prolate shape, which is reversed at large fields, when the droplet becomes oblate again – this re-entrant transition was predicted and observed in [6].

The droplet energy minimization approach [7, 38] shown in blue in Figure 9, as well as experimental observations [6] at large enough magnetic fields ($Bm \gtrsim 70$) predict the droplet undergoing a prolate-oblate transition – reverting back to its pancake-like shape.

We observe a qualitatively similar result in the analysis of Fourier modes A_2 of slightly perturbed ellipsoidal droplets, where in stronger magnetic fields $Bm \gtrsim 50$ the growth increment β_2 becomes negative again, indicating the decay of the $n = 2$ mode and thus allowing the droplet to re-enter its oblate form again.

The difference of the re-entrant field values might have hint at the limits of the ellipsoidal approximation used in deriving the critical field in the energy minimization approach.

6 Conclusion

6.1 Discussion

The development of the boundary element method algorithm for three-dimensional magnetic fluid free interface dynamics allows to validate various relations describing their behavior and may be compared with experimental data, thus providing insight regarding the physical properties of the concentrated phase of magnetic colloids. These colloids can have many interesting properties due to their highly magnetic nature – such as dependence of rheological properties or surface tension on the magnetic field.

The newly created numerical tool has been tested against some theoretical solutions where possible – equilibrium curves of droplet elongation in constant magnetic fields with various relative magnetic permeability μ values, the exponential decay of small elongations under surface tension without external magnetic fields, the dynamical behaviour around the hysteresis bottleneck instability regions, as well as droplet dynamics in various rotating field configurations and the critical fields for oblate–prolate transition. These tests allow to probe the limits of various theoretical approximations and assumptions often used in description of magnetic fluid droplets, for a notable example, the assumption of ellipsoidal shape.

The correspondence of theoretical predictions with numerical results also extends the application limits of the simple magnetic fluid model description of these droplets, which seem to be a rather new kind of soft magnetic matter with *a priori* nontrivial physical properties.

The algorithm has also been shown to be appropriate in prediction of full three-dimensional droplet dynamics with arbitrary droplet-fluid viscosity ratios in uniform fields, both static and rotating up to moderately large droplet deformations. This is important, as experimentally magnetic fluid droplets are not usually axisymmetric and so have to be described carefully in 3D, and can reach viscosity ratios of $\lambda \approx 100$. The algorithm also allows to explore droplet dynamics

in rotating magnetic fields of moderate frequencies, where the fast–rotating field averaging approximation does not hold, which has not been previously possible.

In addition, the algorithm can capture the expected characteristic behaviour of magnetic fluid droplets in rotating magnetic fields, in particular, following the external field at low rotation frequencies and exhibiting a back-and-forth motion at moderately fast fields, similarly to solid magnetic rods or particles, as well as the droplet undergoing the oblate–prolate–oblate transition at fast rotating fields of increasing strength.

However, the algorithm is currently limited in its ability to simulate large deformations of the droplet. It also is unable to simulate a symmetrical appearance of the starfish instability modes without an artificial perturbation of the droplet's shape. The unperturbed starfish instability modes possessed a certain asymmetry both in their angular position and their length as well. In order to speed up the simulation times, the node removal routine in regions of small surface curvature should be implemented, as has been demonstrated previously [31]. Moreover, the existing algorithm version relies on assumptions of uniform surface tension and linear magnetization of the droplet. And finally, the present algorithm cannot handle topological changes of droplets like coalescence or breakup, as well as multiple drops interacting. It is, however, possible to extend the BEM algorithm to these cases[30].

A notable contribution of this work is the numerical confirmation of the main characteristics of magnetic fluid droplet behavior in static and rotating fields. This allows for the study of droplet dynamics in highly non–equilibrium situations not tractable at present by any theoretical approach, as well as exploring various phenomena that may be sensitive to the precise values of multiple physical parameters of either the droplet or its surroundings.

6.2 Main conclusions

- When the "starfish" instability modes of a droplet in a rotating field compete, the mode appearing first may not turn out to be the dominant one.
- Analysis of droplet surface perturbation evolution allows to precisely determine the magnetic field thresholds above which the manisfestation of particular "starfish" instability modes is possible.
- Higher "starfish" instability modes require stronger magnetic fields to appear.
- Fluid magnetic objects can exhibit back-and-forth motion in rotating magnetic fields, similarly to their solid counterparts.
- The model of an infinitely long cylindrical magnetic fluid droplet [43] overestimates the critical field at which the "starfish" instability occurs, possibly due to an underestimate of the capillary forces.
- The simple model of a magnetic fluid droplet is sufficient to capture the various complex surface dynamics of the droplet in external fields, in spite of the additional assumptions of linear magnetic susceptibility and uniform surface tension.

6.3 Thesis

Using simulations of boundary integral equations it is possible to fully describe the three-dimensional free interface dynamics of magnetic fluid droplets.

7 References

[1] S. Chandrasekhar, *Ellipsoidal Figures of Equilibrium*. Yale University Press, Dover, 1969.

[2] G. Taylor, "Disintegration of water drops in an electric field," *Proceedings of the Royal Society of London. Series A. Mathematical and Physical Sciences*, vol. 280, pp. 383–397, July 1964.

[3] R. Rosensweig, *Ferrohydrodynamics*. Dover Books on Physics, Dover Publications, 1985.

[4] V. Drozdova, T. Skrobotova, and V. Chekanov, "Experimental study of the hydrostatics characterizing the interphase boundary in a ferrofluid," *Magnetohydrodynamics*, vol. 15, pp. 12–14, 3 1979.

[5] J. Bacri and D. Salin, "Instability of ferrofluid magnetic drops under magnetic field," *Journal de Physique Lettres*, vol. 43, no. 17, pp. 649–654, 1982.

[6] J.-C. Bacri, A. O. Cebers, and R. Perzynski, "Behavior of a magnetic fluid microdrop in a rotating magnetic field," *Physical Review Letters*, vol. 72, pp. 2705–2708, Apr. 1994.

[7] K. I. Morozov and A. V. Lebedev, "Bifurcations of the shape of a magnetic fluid droplet in a rotating magnetic field," *Journal of Experimental and Theoretical Physics*, vol. 91, pp. 1029–1032, Nov. 2000.

[8] A. Cebers and M. Mayorov, "Structures of interface a bubble and magnetic fluid in a field," *Magnetohydrodynamics*, vol. 16, pp. 231–235, 1980.

[9] A. O. Tsebers and M. M. Maiorov, "Magnetostatic instabilities in plane layers of magnetizable liquids," *Magnetohydrodynamics*, vol. 16, no. 1, pp. 21–28, 1980.

[10] C. Rigoni, G. Beaune, B. Harnist, F. Sohrabi, and J. V. I. Timonen, "Ferrofluidic aqueous two-phase system with ultralow interfacial tension and micro-pattern formation," *Communications Materials*, vol. 3, p. 26, Dec. 2022.

[11] J.-C. Bacri and D. Salin, "Bistability of ferrofluid magnetic drops under magnetic field„" vol. 39, no. 1, pp. 48–50.

[12] A. Cebers, "Virial method of investigation of statics and dynamics of drops of magnetizable liquids," *Magnetohydrodynamics (Engl. Transl.); (United States)*, vol. 21, 7 1985.

[13] S. Afkhami, A. J. Tyler, Y. Renardy, M. Renardy, T. G. St. Pierre, R. C. Woodward, and J. S. Riffle, "Deformation of a hydrophobic ferrofluid droplet suspended in a viscous medium under uniform magnetic fields," *Journal of Fluid Mechanics*, vol. 663, pp. 358–384, Nov. 2010.

[14] J.-C. Bacri and D. Salin, "Dynamics of the shape transition of a magnetic ferrofluid drop," *Journal de Physique Lettres*, vol. 44, no. 11, pp. 415–420, 1983.

[15] J. V. I. Timonen, M. Latikka, L. Leibler, R. H. A. Ras, and O. Ikkala, "Switchable Static and Dynamic Self-Assembly of Magnetic Droplets on Superhydrophobic Surfaces," *Science*, vol. 341, pp. 253–257, July 2013.

[16] F. Serwane, A. Mongera, P. Rowghanian, D. A. Kealhofer, A. A. Lucio, Z. M. Hockenbery, and O. Campàs, "In vivo quantification of spatially varying mechanical properties in developing tissues," *Nature Methods*, vol. 14, pp. 181–186, Feb. 2017.

[17] P. Das, M. Colombo, and D. Prosperi, "Recent advances in magnetic fluid hyperthermia for cancer therapy," *Colloids and Surfaces B: Biointerfaces*, vol. 174, pp. 42–55, 2019.

[18] X. Fan, M. Sun, L. Sun, and H. Xie, "Ferrofluid Droplets as Liquid Microrobots with Multiple Deformabilities," *Advanced Functional Materials*, vol. 30, p. 2000138, June 2020.

[19] X. Fan, X. Dong, A. C. Karacakol, H. Xie, and M. Sitti, "Reconfigurable multifunctional ferrofluid droplet robots," *Proceedings of the National Academy of Sciences*, vol. 117, pp. 27916–27926, Nov. 2020.

[20] R. Kay, C. Katrycz, E. J. Heimlich, and B. D. Hatton, "Programmable droplets: Leveraging digitally-responsive flow fields to actively tune liquid morphologies," *PLoS ONE*, vol. 17, 2022.

[21] C. Pozrikidis, *A practical guide to boundary element methods with the software library BEMLIB*. Chapman & Hall/CRC, 2002.

[22] C. Pozrikidis, *Boundary Integral and Singularity Methods for Linearized Viscous Flow*. Cambridge: Cambridge University Press, 1992.

[23] R. M. Oliveira and J. A. Miranda, "Fully nonlinear simulations of ferrofluid patterns in a radial magnetic field," *Phys. Rev. Fluids*, vol. 5, p. 124003, Dec 2020.

[24] J. D. Sherwood, "Breakup of fluid droplets in electric and magnetic fields," *Journal of Fluid Mechanics*, vol. 188, pp. 133–146, Mar. 1988.

[25] H. A. Stone, J. R. Lister, and M. P. Brenner, "Drops with conical ends in electric and magnetic fields," *Proceedings of the Royal Society of London. Series A: Mathematical, Physical and Engineering Sciences*, vol. 455, pp. 329–347, Jan. 1999.

[26] O. Lavrova, G. Matthies, T. Mitkova, V. Polevikov, and L. Tobiska, "Numerical treatment of free surface problems in ferrohydrodynamics," *Journal of Physics: Condensed Matter*, vol. 18, pp. S2657–S2669, Sept. 2006.

[27] Í. M. Coutinho and J. A. Miranda, "Peak instability in an elastic interface ferrofluid," *Physics of Fluids*, vol. 32, p. 052104, May 2020.

[28] I. Drikis, J.-C. Bacri, and A. Cebers, "Labyrinthine pattern formation in disordered system of the magnetic fluid drops: Numerical simulation," *Magnetohydrodynamics*, vol. 35, pp. 157–169, 01 1999.

[29] A. Z. Zinchenko, M. A. Rother, and R. H. Davis, "A novel boundary-integral algorithm for viscous interaction of deformable drops," *Physics of Fluids*, vol. 9, pp. 1493–1511, June 1997.

[30] A. Z. Zinchenko and R. H. Davis, "Emulsion flow through a packed bed with multiple drop breakup," *Journal of Fluid Mechanics*, vol. 725, pp. 611–663, June 2013.

[31] V. Cristini, J. Bławzdziewicz, and M. Loewenberg, "An Adaptive Mesh Algorithm for Evolving Surfaces: Simulations of Drop Breakup and Coalescence," *Journal of Computational Physics*, vol. 168, pp. 445–463, Apr. 2001.

[32] X. Ni, B. Zhu, B. Wang, and B. Chen, "A level-set method for magnetic substance simulation," *ACM Transactions on Graphics*, vol. 39, Aug. 2020.

[33] W. C. Jesus, A. M. Roma, and H. D. Ceniceros, "Deformation of a sheared magnetic droplet in a viscous fluid," *Commun. Comput. Phys*, vol. 24, pp. 332–355, 2018.

[34] C. S. Peskin, "Flow patterns around heart valves: A numerical method," *Journal of Computational Physics*, vol. 10, no. 2, pp. 252–271, 1972.

[35] X. Li, Z.-Q. Dong, P. Yu, X.-D. Niu, L.-P. Wang, D.-C. Li, and H. Yamaguchi, "Numerical investigation of magnetic multiphase flows by the fractional-step-based multiphase lattice Boltzmann method," *Physics of Fluids*, vol. 32, p. 083309, Aug. 2020.

[36] S. Afkhami and Y. Renardy, "Ferrofluids and magnetically guided superparamagnetic particles in flows: a review of simulations and modeling," *Journal of Engineering Mathematics*, vol. 107, pp. 231–251, Dec. 2017.

[37] D. Das and D. Saintillan, "Electrohydrodynamics of viscous drops in strong electric fields: Numerical simulations," *Journal of Fluid Mechanics*, vol. 829, pp. 127–152, Oct. 2017. arXiv: 1612.02070.

[38] J. Erdmanis, G. Kitenbergs, R. Perzynski, and A. Cēbers, "Magnetic micro-droplet in rotating field: numerical simulation and comparison with experiment," *Journal of Fluid Mechanics*, vol. 821, pp. 266–295, June 2017.

[39] A. Stikuts, R. Perzynski, and A. Cēbers, "Spontaneous order in ensembles of rotating magnetic droplets," *Journal of Magnetism and Magnetic Materials*, vol. 500, p. 166304, Apr. 2020.

[40] E. Blūms, A. O. Cebers, and M. M. Maĭorov, *Magnetic fluids*. Berlin ; New York: Walter de Gruyter, 1997.

[41] I. R. Siqueira, R. B. Rebouças, T. F. Oliveira, and F. R. Cunha, "A new mesh relaxation approach and automatic time-step control method for boundary integral simulations of a viscous drop," *International Journal for Numerical Methods in Fluids*, vol. 84, pp. 221–238, June 2017.

[42] V. G. Bashtovoi, S. G. Pogirnitskaya, and A. G. Reks, "Determination of the shape of a free drop of magnetic fluid in a uniform magnetic field," *Magnetohydrodynamics (Engl. Transl.); (United States)*, vol. 23:3, 1 1988.

[43] S. Lācis and A. Cēbers, "Magnetic fluid free surface instabilities in high frequency rotating magnetic fields," *Brazilian Journal of Physics*, vol. 25, pp. 101–111, 1995.